



**HAL**  
open science

## Understanding fracture mode-mixity and its effects on bond performance

Bamber Blackman, Fengzhen Sun, Sofia Teixeira de Freitas, Silvio de Barros, Marcio Moreira Arouche, Alojz Ivankovic

► **To cite this version:**

Bamber Blackman, Fengzhen Sun, Sofia Teixeira de Freitas, Silvio de Barros, Marcio Moreira Arouche, et al.. Understanding fracture mode-mixity and its effects on bond performance. *Advances in Structural Adhesive Bonding*, Elsevier, pp.579-613, 2023, 978-0-323-91214-3. 10.1016/B978-0-323-91214-3.00015-6 . hal-04239740

**HAL Id: hal-04239740**

**<https://hal.science/hal-04239740v1>**

Submitted on 13 Oct 2023

**HAL** is a multi-disciplinary open access archive for the deposit and dissemination of scientific research documents, whether they are published or not. The documents may come from teaching and research institutions in France or abroad, or from public or private research centers.

L'archive ouverte pluridisciplinaire **HAL**, est destinée au dépôt et à la diffusion de documents scientifiques de niveau recherche, publiés ou non, émanant des établissements d'enseignement et de recherche français ou étrangers, des laboratoires publics ou privés.

## CHAPTER 18

### Understanding fracture mode-mixity and its effects on bond performance

**Bamber Blackman<sup>1</sup>, Fengzhen Sun<sup>2</sup>, Sofia Teixeira De Freitas<sup>3</sup>, Silvio de Barros<sup>4</sup>, Marcio Moreira Arouche<sup>3</sup> & Alojz Ivankovic<sup>5</sup>**

*<sup>1</sup> Department of Mechanical Engineering, Imperial College London, South Kensington Campus, London, UK; <sup>2</sup> Tongji University, Shanghai, China; <sup>3</sup> TU Delft, The Netherlands; <sup>4</sup> LINEACT CESI Engineering School, Paris, France; <sup>5</sup> University College Dublin, Dublin, Ireland.*

**Abstract:** This chapter discusses the mixed-mode loading of adhesive joints. The importance of mixed-mode loading is firstly introduced and then test methods commonly used to measure the mixed-mode fracture resistance of adhesive joints are presented and briefly discussed. The approaches to determine the fracture resistance are briefly reviewed and then the partitioning of mixed-mode fracture energies is discussed. The limitations of the local singular field and global approaches to mixed-mode partitioning are discussed and the use and application of a semi-analytical cohesive zone analysis partitioning scheme is evaluated. The limitations of the global partitioning approach are further discussed in the context of developing a scheme to design and analyse adhesive joints with dissimilar adherends (a bi-material interface). A longitudinal strain criterion is proposed in addition to the matching of flexural rigidities and the approach is validated numerically. Finally, the practical issues of crack stability, failure path selection and the use of mixed-mode failure envelopes is considered.

**Key Words:** Adhesive joint; mode-mixity; partitioning; global approach, local approach, cohesive zone model, bi-material interface.

#### 17.1 Introduction

The use of structural adhesives to join engineering components and structures has become very popular due to the many advantages which structural adhesive bonding brings- namely the avoidance of the need to drill holes or introduce local damage to the adherends, the improved stress distribution of adhesively bonded joints compared with mechanically

fastened or welded joints, the ability to join dissimilar adherends and the improvement in structural rigidity, reduction of vibration, and improved fatigue resistance all make structural adhesive bonding a very highly employed joining technique.

To optimize joint performance, many studies [1,2] have shown that tensile opening forces (mode I) should be minimized and that in-plane shear forces (mode II) should be maximized. For this reason, tensile butt joints are typically avoided, in favour of joints loaded in shear such as the single or double lap joint. To further optimize joint performance, stress concentrations should be minimized by employing tapered adherends so the tapered double lap joint has superior performance to its non-tapered equivalent.

To measure adhesive joint performance, extensive use has been made of fracture mechanics since the pioneering initial studies by Ripling, Mosovoy and Patrick in the 1960s [3]. Their work focused mainly on mode I loading of joints employing metallic adherends and led to the popular ASTM standard [4]. As structural joint designs were improved, there was increased interest in mode II and mixed-mode loading (i.e. combinations of modes I, II and III acting together) and many workers explored test methods which combined modes- most commonly modes I and II. Although there have been many notable contributors to the development of the understanding of the mixed-mode fracture behaviour in adhesive joints e.g. [5–7], there is a lack of standardized tests developed specifically for these structures.

To analyse mixed-mode fracture tests, most workers have followed the energy release rate ( $G$ ) approach and have combined this with beam theory methods to determine the rate of change of compliance  $C$  with crack length  $a$ , i.e. to determine  $dC/da$ . This is then combined with the Irwin-Kies equation [8] to calculate the critical value of  $G$  for fracture,  $G_c$ . Initially, Linear Elastic Fracture Mechanics (LEFM) theory was followed, where one assumption is that any in-elastic deformation is limited in size to a very small zone at the crack tip and that the specimen behaves in a linear-elastic manner overall. Such assumptions are valid for brittle adhesives, but as adhesives have been manufactured with greatly improved toughness or ductility, the size of the in-elastic deformation zone at the crack tip has greatly increased, requiring the use of cohesive zone models to combine the approaches of fracture mechanics and classical strength of materials. The use of cohesive zone models and the concept of the cohesive zone length (damage length) has become increasingly important in the analysis of fracture in adhesively bonded joints under mixed-mode loading, as will be discussed in more detail later in this chapter, as well as in Chapter 37 (Jackson) with digital image correlation (DIC) methods.

## 17.2 Brief summary of test methods to introduce mixed-mode loading

The accurate measurement of the fracture energy ( $G_c$ ) is one key research campaign for characterization of the fracture behaviour of laminated composites and adhesively bonded interfaces. Over the last few decades, many methodologies and data reduction schemes have been proposed to quantify the fracture energy for the mode I, mode II and mixed I/II mode loading [9]. Double cantilever beam (DCB) specimens loaded with pure bending moments provide a very accurate and robust way to determine the mode I fracture toughness ( $G_{Ic}$ ) without the need of measuring crack lengths, however, this method does rely on the use of a specially designed loading jig [10]. Instead, specimens loaded with a

shear load are more often adopted, but this gives rise to the problem of determination of the crack length. End notched flexure (ENF) tests using three-point bending apparatus are extensively employed to measure the mode II fracture toughness ( $G_{IIc}$ ) due to the test convenience, however, the crack growth in the specimens are intrinsically unstable and thus only initiation values of  $G_{IIc}$  are usually obtained [11]. Another way to determine the value of  $G_{IIc}$  is by using the end-loaded split (ELS) specimens, which are tested in a sliding clamp that only allows the specimen to slide freely in the horizontal direction, and the crack growth is relatively stable [12]. In addition, prior to the ELS test, a correction to the end clamping needs to be determined.

In practice, very rarely does failure in bonded joints occur under pure mode loading conditions, and crack growth under a combination of opening and shear modes is more commonly encountered, making it necessary to characterize the fracture behaviour of adhesive joints under mixed mode loading. Mixed mode flexure (MMF) also known as single leg bending (SLB) and the fixed ratio mixed mode (FRMM) specimens are convenient choices to complement the results obtained with the pure mode tests. The MMF configuration is very similar to the ENF test, and it is tested using a three-point bending rig, but only the upper arm at one end of the specimen is loaded. The FRMM geometry employs the same clamping arrangement as the mode II ELS test, but only one arm is loaded in this case. Symmetric MMF and FRMM specimens yield a constant mode-mixity  $G_{II}/G$  of 3/7.

Apart from the constant mode-mixity tests, a range of mode-mixity can be obtained by altering the relative thickness of the substrates such as the asymmetric DCB (ADCB) and asymmetric FRMM (AFRMM) specimens, although this raises the question of how to partition the mode-mixity correctly, which will be discussed in detail in the following section. ADCB and AFRMM are the generalization of the standard DCB and FRMM specimens using different beam thickness or different materials for the substrates. The specimens are manufactured and tested in the same manner as the DCB and FRMM test. ADCB specimens are simpler to test than AFRMM specimens, but the achievable range of mode-mixity is much more limited in the ADCB than the AFRMM case.

Another strategy to induce mixed-mode fracture is loading a symmetric adhesive joint with an apparatus designed to apply different load combinations such as those used in mixed mode bending (MMB) [13], Arcan fixtures [14] and the rig developed by Fernlund and Spelt [15]. The MMB test is the only standardized mixed mode I/II test available [16]. Although this standard was initially developed for unidirectionally fibre reinforced polymer (FRP) composites, it has been successfully used to test multidirectional FRPs and adhesive joints. The MMB test covers a wide range of mode I to mode II loadings by adjustment of the loading and lever fulcrum positions in the test apparatus [13]. This type of test combines opening and in-plane sliding displacement modes, and the applied loading usually is treated as the superposition of the applied loadings of the DCB and ENF tests. Its particular advantage is that a range of mixed-mode I/II load cases can be studied without having to change the specimen geometry, but it does require a complex fixture and bonded steel hinged tabs, which may introduce a geometrical nonlinearity.

Another mixed-mode loading apparatus was introduced by Fernlund and Spelt [15]. The load jig consists of a link-arm system which allows the force acting on the upper and lower substrates of the test specimen respectively, to be varied by altering the load jig geometry. The links in the load jig were connected to each other with dowel pins to facilitate the

geometry change. The nominal phase angle of loading is independent of the crack length of the specimen, and it also allows the mode ratios from pure mode I to pure mode II. Important features are that all mode ratios can be generated with a single equal-adherend DCB specimen, and the mode ratio is independent of crack length. Recently, Costa et al. [17] developed a more compact apparatus with the same basis proposed by Fernlund and Spelt. All the mixed-mode and classical models (ATDCB, SLB, DCB and ENF) have further validated the results obtained with the new apparatus, providing a clear confirmation that valid mixed-mode results were obtained.

Arcan et al. [14] proposed a biaxial fixture, commonly known as the Arcan fixture, to produce biaxial states of stress. The compact nature of the Arcan fixture enables the shear properties in all in-plane directions to be obtained in a relatively simple manner. Various mixed mode combination can be achieved by rotating the loading direction. However, although the Arcan test covers all the mixed-mode ratios including the pure mode-I to mode-II, the results can only be obtained by a numerical (finite element) analysis, which involves the singularity at the crack tip. The cracked-lap shear (CLS) was also an attempt to construct a mixed-mode testing approach [18]. One distinctive feature of the CLS is the eccentric loading path that leads to geometrical nonlinearity [19], and thus large deflections have to be considered in analytical and numerical analyses. Due to these limitations, it is used only in few cases.

## 17.3 Mixed-mode partitioning schemes

### 17.3.1 Introduction

The mixed-mode loading situation raises fundamental questions which are not relevant to the pure mode case. For example, to what extent do the two loading modes interact when applied simultaneously to modify the resistance of the joint from that which would be predicted from a simple linear addition of the separate mode contributions? Indeed, it is frequently observed that such a linear addition is a poor descriptor of mixed-mode fracture resistance, and that a stronger interaction exists [20] so to define the correct degree of interaction (fracture criterion), it is important to be able to partition the total loading correctly into its constituent parts. In terms of fracture energy, the mixed-mode fracture resistance  $G_c$  must be partitioned into the mode I and mode II components.

### 17.3.2 Local and global partitioning schemes

Attempts to partition mixed-mode loading into pure mode components have traditionally taken either a local or a global approach. In the local approach, the stress singularity at the crack tip is assumed to control fracture and this requires that the region controlled by the singular field (K-dominant zone) engulfs the crack tip process zone (plastic and/or damage zone). The singular field stress distributions are determined at the crack tip and these are partitioned into the Mode I and II components,  $K_I$  and  $K_{II}$ , which can then be written in terms of the associated energy release rate components,  $G_I$  and  $G_{II}$  respectively. In the

global approach, the bending moments applied to the specimen are considered but the details of the local stress or strain fields ahead of the crack tip are neglected. Williams [21] proposed that these applied moments could be partitioned into components which induce pure mode I ( $M_I$ ) and pure mode II ( $M_{II}$ ). Figure 1 shows a cracked beam-like geometry subjected to pure bending moments of  $M_I$  on the upper beam and  $kM_I$  on the lower beam [22]. The upper beam has a thickness of  $h_1$  and the lower beam a thickness of  $h_2$ , and the ratio of heights,  $\gamma = h_1/h_2$ .

Local and global partitioning approaches have been reviewed by Conroy et al. [22], and an application of the global approach is discussed further in section 17.4. As is shown in Figure 2 (a), when the test specimen has a symmetric geometry, as is the case for the mixed-mode bending (MMB) specimen, then the local and global partitioning approaches produce identical results for the applied mixed-mode partition ratio,  $G_{II}/G$ . Note that for  $\gamma = 1$ , when the applied moment ratio,  $k = -1$  then pure mode I loading is obtained and when  $k = 1$  then pure mode II is obtained. However, as is shown in Figure 2(b), for an unsymmetric geometry, in this case the AFRMM specimen, then the local and global partitioning approaches produce very different results. Figure 2(b) shows the mixed-mode partition ratio  $G_{II}/G$  as a function of the beam height ratio  $\gamma$ , where the two approaches only agree when  $\gamma = 1$ . It is noteworthy therefore that if only symmetric specimens are used, the two partitioning approaches produce identical results in monolithic specimens.

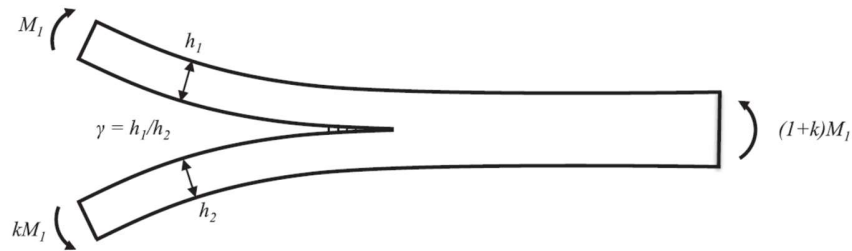


Figure 1. Beam-like geometry subjected to pure bending moments ( $M_I$  and  $kM_I$ ) [22].

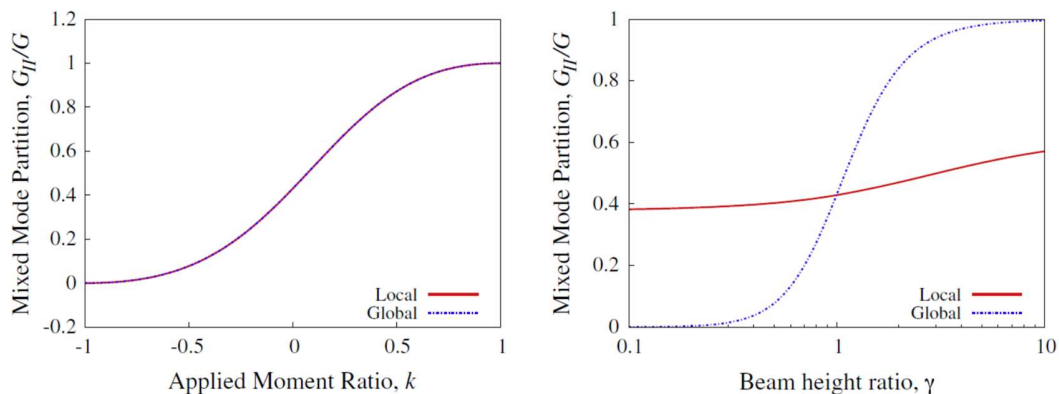


Figure 2. Local and global partitioning: (a) symmetric specimens e.g. MMB; (b) asymmetric specimens e.g. AFRMM [22].

### 17.3.3 A damage-based partitioning scheme

For highly fracture resistant materials, including joints bonded with toughened adhesives, the length of the fracture process zone (the cohesive zone) can be significantly larger than the extent of the singular field and for these materials the global approach has traditionally found greater success. However, Conroy et al. [22] noted from their numerical studies that as the degree of damage increased, i.e. as the size of the cohesive zone increased, then the global partitioning approach becomes more accurate. Conversely, as the amount of damage decreased then the local partitioning approach becomes more accurate. Conroy et al. [22] proposed a damage-dependent partitioning method which was termed the semi-analytical cohesive analysis (SACA) ref which is now discussed.

Conroy et al. [22] proposed that the partitioning approach should acknowledge the state of damage in the specimen and they allowed this to be scaled, via a singularity factor  $f$ , between a lower bound given by the local solution and an upper bound given by the global solution, where  $f$  was given by:

$$f = \frac{\left(\frac{G_{II}}{G}\right) - \left(\frac{G_{II}}{G}\right)_W}{\left(\frac{G_{II}}{G}\right)_{HS} - \left(\frac{G_{II}}{G}\right)_W} \quad (17.1)$$

where  $(G_{II}/G)_W$  and  $(G_{II}/G)_{HS}$  are the mixed-mode ratios given by the global and local solutions respectively and  $(G_{II}/G)$  is the predicted mixed-mode partition ratio according to this semi-analytical cohesive analysis (SACA) method. To employ the SACA method, a normalized damage length parameter was defined for the specimen,  $l_{nd}$ , where this is given by:

$$l_{nd} = \frac{l_{cz}}{a_c} \quad (17.2)$$

where  $l_{cz}$  is the cohesive zone length and  $a_c$  is the smallest characteristic dimension of the specimen. The cohesive zone lengths in modes I and II were determined analytically and the singularity factor was then given by eqn 17.3 or 17.4, depending upon whether the value of  $l_{nd}$  was less than 0.3.

$$f = 1 \quad \text{if } l_{nd} \leq 0.3 \quad (17.3)$$

$$f = 0.9682e^{-0.24l_{nd}} + 0.0983e^{-0.2l_{nd}} \quad \text{otherwise} \quad (17.4)$$

Based upon eqns 17.3 and 17.4, partitioning via the local singular field approach was considered accurate for cohesive zone lengths up to 30% of the smallest characteristic



length. The singularity factor  $f$  was dependent upon material properties and specimen geometry. Conroy et al. [22] applied the method to various test cases based upon composite materials in the literature with excellent results. The method is evaluated for a structural adhesive joint in the next section.

#### 17.3.4 Evaluation and discussion of mixed-mode partitioning

Mixed-mode partitioning schemes were investigated experimentally by Alvarez et al. [23] for structural adhesive joints in which carbon-fibre reinforced composite adherends had been bonded with a toughened aerospace film adhesive grade AF163-2 OST. These authors employed various test specimens including the ADCB, the FRMM and the AFRMM. The experimental results were partitioned according to the global approach, and according to two forms of the local approach: firstly one based upon the crack tip element (CTE) method of Davidson et al. [24], which was termed the singular field (CTE-SF) and the second method, a non-singular field (CTE-NSF) version of Davidson's method. They also explored the use of the SACA method.

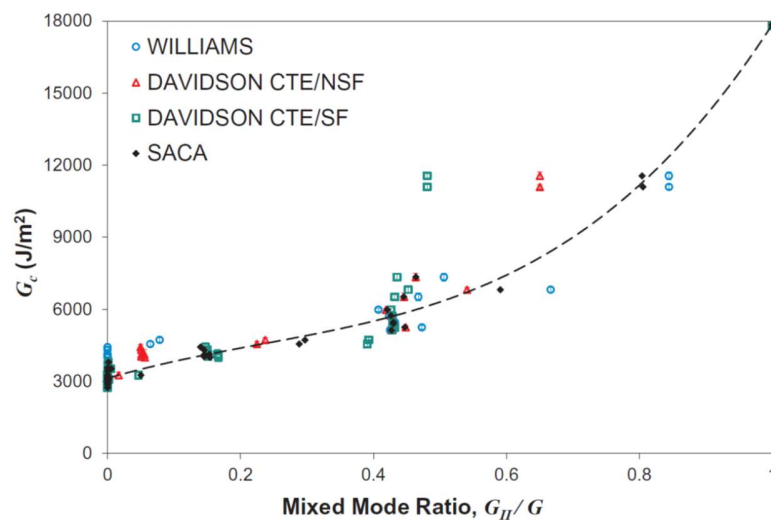


Figure 3. Comparison of the failure locus obtained from the experimental results partitioned via the global approach (Williams [21]), the singular and non-singular field versions of Davidson's analysis CTE/NSF and CTE/SF and the SACA method [23].

Alvarez et al. [23] found that for this relatively tough adhesive joint, the global partitioning approach [21] was generally accurate across the range of mixed-mode ratios ( $G_{II}/G$ ) attained but showed the largest percentage errors at the smallest mixed-mode ratios. Additionally, as it has frequently been remarked in the literature, the global partitioning approach is anomalous for the ADCB test, where it predicts ( $G_{II}/G$ ) = 0, i.e. mode I, for all arm thickness ratios. The local approach via Davidson's CTE-SF method was accurate at the smallest mixed-mode ratios and Davidson's CTE-NSF method was accurate at intermediate ratios, but both became non-physical at higher mixed-mode ratios, e.g. for



$(G_{II}/G) > 0.5$ . The SACA method, in which the singularity factor,  $f$ , was determined for the adhesive joint based upon the material properties of the adhesive and the adherends and the specimen geometry, gave the most accurate mixed mode partitioning across the entire range  $0 < (G_{II}/G) \leq 1$ . In Figure 3, the mixed-mode failure envelope was drawn using the B-K criterion. Note that failure envelopes are discussed in more detail in section 17.5 of the present chapter.

#### 17.4 Application of global partitioning to mixed-mode bi-material interface joints.

In this section, the mixed-mode fracture behavior of a bi-material adhesively bonded joint is investigated. The strain-based method (SBM) is described, evaluated and tested on a composite-to-metal bonded joint using the mixed-mode bending (MMB) test.

##### 17.4.1 Longitudinal strain-based criterion

###### 17.4.1.1. Strain energy release rate

The strain energy release rate (SERR) is one of the most important parameters to consider for characterizing the fracture behavior of cracked structures. For linear elastic behaviour, the total SERR can be obtained by the balance of fracture energy through the following equation:

$$G = \frac{1}{B} \left( \frac{\delta U_e}{\delta a} - \frac{\delta U_s}{\delta a} \right) \quad (17.5)$$

where  $B$  is the width of the specimen,  $U_e$  is the external work performed,  $U_s$  is the strain energy and  $a$  is the crack length. The analysis considers a region ABCD mechanically affected by the presence of a crack under pure bending moments, as shown in Figure 4.

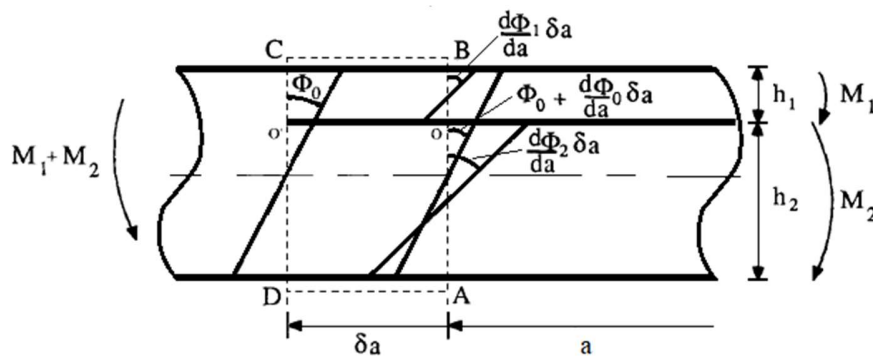


Figure 4. Beam analysis under pure bending moments [25].

The upper and lower arm thickness are  $h_1$  and  $h_2$ , and the bending moments applied on the upper and lower arms are  $M_1$  and  $M_2$ , respectively. The angles  $\Phi_0$ ,  $\Phi_1$  and  $\Phi_2$  represent the slopes of the beam, upper arm and lower arm, respectively. When the crack grows a length  $\delta a$  from O on section AB to O' on section CD, the external work is:

$$\frac{\delta U_e}{\delta a} = M_1 \left( \frac{\delta \Phi_1}{\delta a} - \frac{\delta \Phi_0}{\delta a} \right) + M_2 \left( \frac{\delta \Phi_2}{\delta a} - \frac{\delta \Phi_0}{\delta a} \right) \quad (17.6)$$

For pure bending, the change in angle is given by:

$$\frac{\delta \Phi}{\delta a} = \frac{M}{EI} \quad (17.7)$$

where  $M$  is the moment,  $E$  is the flexural modulus and  $I$  is the second moment of area. Similarly, the strain energy is:

$$\frac{\delta U_s}{\delta a} = \frac{M_1^2}{2E_1 I_1} + \frac{M_2^2}{2E_2 I_2} - \frac{(M_1 + M_2)^2}{2E_{eq} I_{eq}} \quad (17.8)$$

where  $E_1$ ,  $I_1$ ,  $E_2$ ,  $I_2$ ,  $E_{eq}$  and  $I_{eq}$  are the flexural longitudinal moduli and second moments of the area in the section of the crack tip of the upper arm, lower arm and total specimen, respectively. Substituting (17.6) and (17.8) in (17.5), it can be reduced to the equation of the total fracture energy:

$$G = \frac{1}{2B} \left( \frac{M_1^2}{E_1 I_1} + \frac{M_2^2}{E_2 I_2} - \frac{(M_1 + M_2)^2}{E_{eq} I_{eq}} \right) \quad (17.9)$$

Equation (17.9) allows determining the total fracture energy of a crack between two arms. However, it is essential to the characterization of the mechanical behavior to define the contribution of mode I and mode II fracture.

#### 17.4.1.2. Williams' global partitioning approach

Williams [21] proposed a partitioning method (WM) based on the assumptions that: (i) pure mode I exists when opposite moments act on the joint arms; and (ii) pure mode II is obtained when the curvature in the two arms are the same. This means:

$$M_1 = M_{II} - M_I \quad (17.10)$$

$$M_2 = \psi M_{II} + M_I \quad (17.11)$$

Where the bending stiffness ratio between upper and lower arms is:

$$\psi = \frac{E_2 I_2}{E_1 I_1} \quad (17.12)$$

Substituting Equations (17.10) and (17.11) in Equation (17.9), the equation of the total fracture energy can be reduced to:

$$G = \frac{1}{2B} \left[ M_I^2 \left( \frac{\psi + 1}{E_2 I_2} \right) + M_{II}^2 \left( \frac{\psi + \psi^2}{E_2 I_2} - \frac{(1 + \psi)^2}{E_{eq} I_{eq}} \right) \right] \quad (17.13)$$

Notice that no cross-product term is observed. Therefore, the partitioning can be obtained by rewriting Equation (17.3) as function of  $M_I$  and  $M_{II}$ :

$$f(M_I, M_{II}) = f_I(M_I) + f_{II}(M_{II}) \quad (17.14)$$

$G_I$ ,  $G_{II}$  and the total  $G$  are then given by:

$$G_I = \frac{M_I^2}{2B} \left( \frac{\psi + 1}{E_2 I_2} \right) \quad (17.15)$$

$$G_{II} = \frac{M_{II}^2}{2B} \left( \frac{\psi + \psi^2}{E_2 I_2} - \frac{(1 + \psi)^2}{E_{eq} I_{eq}} \right) \quad (17.16)$$

$$G = G_I + G_{II} \quad (17.17)$$

Finally, substituting Equation (17.10) and (17.11) in (17.15) and (17.16), the mode I and mode II SERR can be written as:

$$G_I = \frac{(\psi M_1 - M_2)^2}{2B(\psi + 1)^2} \left( \frac{1}{E_1 I_1} + \frac{1}{E_2 I_2} \right) \quad (17.18)$$

$$G_{II} = \frac{(M_1 + M_2)^2}{2B(\psi + 1)} \left( \frac{1}{E_1 I_1} - \frac{(\psi + 1)}{E_{eq} I_{eq}} \right) \quad (17.19)$$

Analytical models based only on simple beam analysis do not properly describe the crack propagation mechanism [26]. The two arms are not fixed against rotation at the delamination tip as assumed in simple beam analysis. Instead, they rotate slightly due to the elastic support that they provide one another. Such effects arise as a result of shear deformation and deflection at the crack tip, large deflections of the arm and stiffening of the arms due to the presence of the end-blocks. Williams [27] proposed a correction factor, based on Kanninen's [28] elastic foundation model, for accounting these various effects in the mode I fracture. Wang and William [29] tested the same correction factor for mode II fracture component. The incorporation of crack tip correction factors in the beam model, Equations (17.18) and (17.19), resulted in the so-called corrected beam theory (CBT). In this model, an effective crack length value is used to account for the contribution to the energy release rate from shear deformations.

The works of Williams [20], Hashemi et al. [30] and Ducept et al. [31] indicated that CBT produces reliable values for the total fracture energy and partitioning ratio of symmetric cracks. However, Ducept et al. [32] showed that WM does not provide reliable results of the fracture mode partitioning of cracks between asymmetric arms. The assumptions for the pure modes do not describe with precision the interaction between

mode I and mode II fracture. Therefore, it is not recommended for the characterization of asymmetric cracks.

### 17.4.1.3. Strain-based partitioning method

The strain-based method (SBM) [25,33] introduced a new criterion for the fracture mode partitioning. The main difference in comparison with the WM lies on the condition for pure mode I: it incorporates the condition of strain equivalence for mode pure mode I, identified by Ouyang [34] and confirmed by Wang et al. [35]. In the case of pure mode II, similarly to WM, the SBM assumes that it is produced when both arms have the same curvature, as observed by Mollón et al. [36]. Therefore, the partitioning assumptions become: (i) the longitudinal strain distribution at the faying surfaces of both arms must be identical in order to produce pure mode I; and (ii) pure mode II is obtained when the curvature in the two arms are the same. This gives:

$$M_1 = M_{II} - M_I \quad (17.20)$$

$$M_2 = \psi M_{II} + \beta M_I \quad (17.21)$$

Where the longitudinal strain ratio between upper and lower arms is:

$$\beta = \frac{E_2 h_2^2}{E_1 h_1^2} \quad (17.22)$$

Substituting Equations (17.20) and (17.21) in Equation (17.9), the total SERR is obtained:

$$G = \frac{1}{2B} \left[ \begin{array}{l} M_I^2 \left( \frac{\psi + \beta^2}{E_2 I_2} - \frac{(\beta - 1)^2}{E_{eq} I_{eq}} \right) + M_{II}^2 \left( \frac{\psi + \psi^2}{E_2 I_2} - \frac{(1 + \psi)^2}{E_{eq} I_{eq}} \right) + \\ M_I M_{II} \left( \frac{2\psi\beta - 2\psi}{E_2 I_2} - \frac{2(1 + \psi)(\beta - 1)}{E_{eq} I_{eq}} \right) \end{array} \right] \quad (17.23)$$

Equation (17.23) shows that the mode I fracture energy affects the mode II fracture energy and vice-versa. Consequently, the equation can only be written in the form of:

$$f(M_I, M_{II}) = f_I(M_I) + f_{II}(M_{II}) + f_c(M_I, M_{II}) \quad (17.24)$$

Equation (17.24) displays a coupling function  $f_c(M_I, M_{II})$  beyond the functions of pure mode I and pure mode II –  $f_I(M_I)$  and  $f_{II}(M_{II})$ , respectively. This implies that the fracture mode partitioning is obtained when the coupling function  $f_c(M_I, M_{II})$  is zero. This is achieved in the condition of  $\beta = 1$ . Therefore, the specimen design condition of longitudinal strain equivalence has to be satisfied. It means:

$$E_1 h_1^2 = E_2 h_2^2 \quad (17.25)$$

In this case, the mode I and mode II equations of fracture energy are the same as in WM – Equations (17.18) and (17.19). However, WM does not reinforce any specific specimen design since it was derived for symmetric specimens in which  $\beta$  is always equal to 1. It ignores the coupling function that contributes to the total fracture energy. This is the reason why WM is inaccurate if applied to asymmetric specimens where the longitudinal strain-based design criterion is not applied ( $\beta \neq 1$ ).

## 17.4.2 Application in MMB test in composite-to-metal bonded joints.

### 17.4.2.1. Mixed-mode bending (MMB) test

Reeder and Crews [36] developed the mixed-mode bending (MMB) test method as a combination of the DCB and the ENF tests. In the MMB test, a load (P) is applied through a roller attached to a lever and loaded just above the mid-plane of the test specimen. The test loading is decomposed into opening ( $P_I$ ) and shear ( $P_{II}$ ) loadings in a constant ratio determined by the lever length (c). The original procedure was later redesigned in order to minimize geometrical nonlinearity effects [37] and to take into account the weight of the lever ( $P_g$ ) and the distance of the lever center of gravity ( $c_g$ ) [38]. Chen et al. [39] proposed a modification to the test apparatus in order to avoid preloading on the specimens caused by the weight of the lever. The MMB test scheme is shown in Figure 5. The MMB test has proved to be an easy and reliable method for measuring a wide range of mixed-mode ratios with only one specimen geometry [31,40]. The loads applied to the specimen are shown in Figure 6.

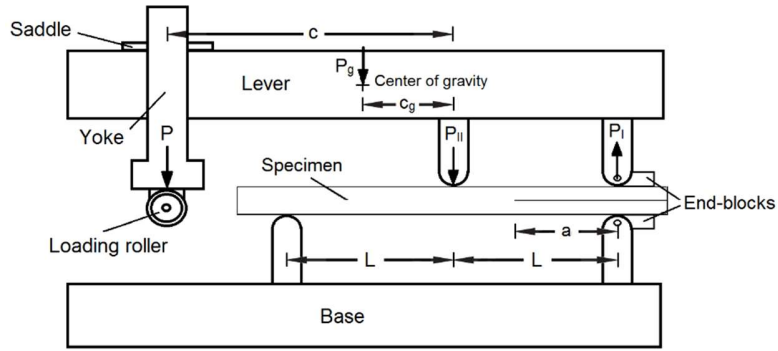


Figure 5. MMB test scheme.

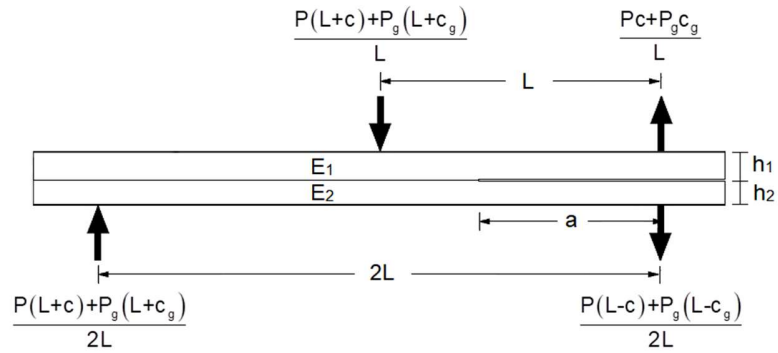


Figure 6. MMB specimen free body diagram.

The resulting bending moments are:

$$M_1 = \frac{Pc + P_g c_g}{L} a \quad (17.26)$$

$$M_2 = \frac{P(L - c) + P_g(L - c_g)}{2L} a \quad (17.27)$$

Then, the mode I and mode II SERR of an MMB test specimen can be obtained by replacing Equations (17.24) and (17.25) in Equations (17.18) and (17.19).



#### 17.4.2.2. Numerical model

A virtual mixed-mode bending (MMB) test was chosen to evaluate the SBM. The geometric features of the bi-dimensional model are 70 mm half-span ( $L$ ) and 50 mm crack length ( $a$ ). The upper and lower arm thicknesses ( $h_1$  and  $h_2$ , respectively) and materials ( $E_1$  and  $E_2$ , respectively) are the parameters varied in the analysis [25].

#### 17.4.2.3. Asymmetric crack within the same material

The first parametric study was performed on an asymmetric crack within the same material. Both arms have elastic modulus ( $E_1$  and  $E_2$ ) of 70 GPa and Poisson's ratio ( $\nu_1$  and  $\nu_2$ ) of 0.33. In order to verify the influence of the fracture mode ratio in the accuracy of the analytical methods, three different conditions were considered: low ( $c = 117$  mm), intermediate ( $c = 61$  mm) and high ( $c = 42$  mm) mode II ratio. Table 1 shows the three cases of geometrical asymmetry. The upper arm thickness ( $h_1$ ) is varied in a wide range of geometries applied to the MMB test specimen while the lower arm thickness ( $h_2$ ) remains 3.0 mm. The crack length is kept at 50 mm and the test load ( $P$ ) is 100 N.

Table 1. Study cases of geometrical asymmetry.

Case	Lever length, $c$ (mm)	$h_1$ (mm)	$h_2$ (mm)	$E_1; E_2$ (GPa)	$\nu_1; \nu_2$
1	117	$1.5 < h_1 < 6.0$	3.0	70	0.33
2	61	$1.5 < h_1 < 6.0$	3.0	70	0.33
3	42	$1.5 < h_1 < 6.0$	3.0	70	0.33

Analytical and numerical results of the total fracture energy ( $G$ ) are presented in Figure 7. Figures 7a, 7b and 7c show the three cases of low (case 1), intermediate (case 2) and high (case 3) mode II fracture, respectively. Overall, the total fracture energy obtained from analytical solutions based on beam analysis are in very good agreement with the numerical results.

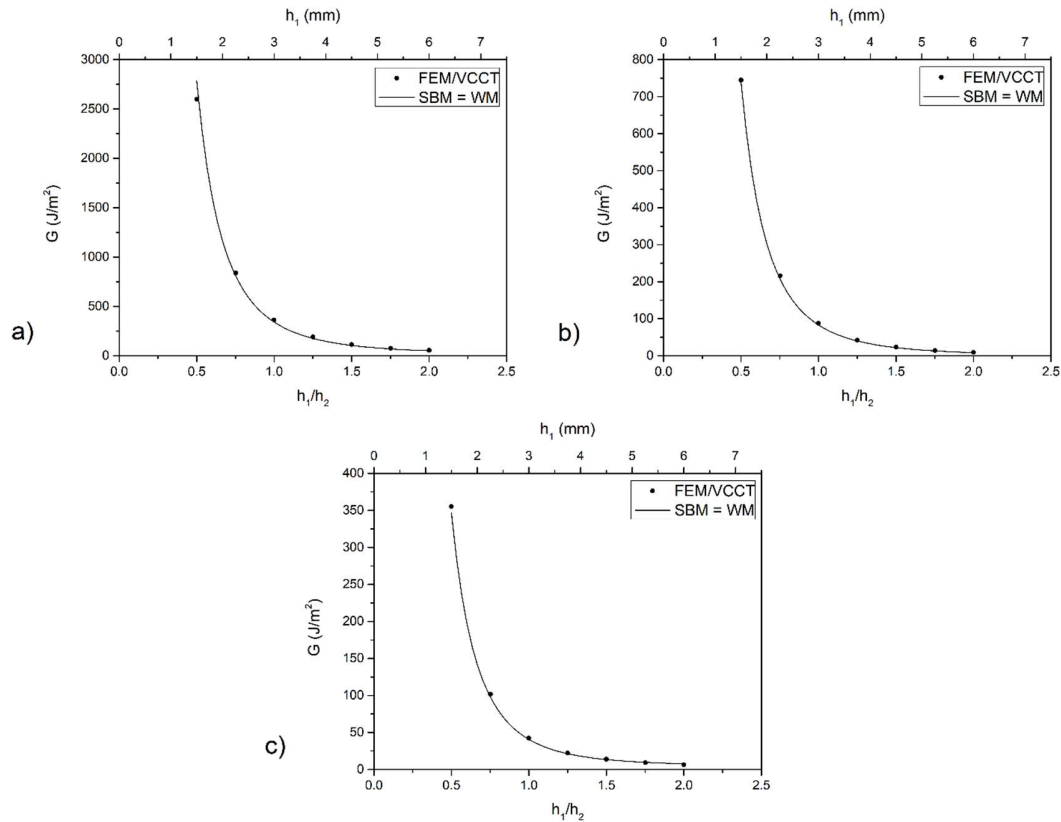


Figure 7. Total fracture energy with the variation of the specimen thickness: cases (a) 1 – low, (b) 2 – intermediate and (c) 3 – high mode II [25].

Figure 8 shows the analytical and numerical fracture mode ratio ( $G_{II}/G$ ). Notice that the SBM is applied only when the specimen design condition is satisfied ( $\beta = 1$ ) and, for this condition, gives the same result of WM. Figure 8a shows the results for low mode II (case 1). When  $\beta = 1$ , the crack is symmetric ( $h_1/h_2 = 1$ ) and both analytical methods show good agreement with numerical results. As  $\beta$  differs from 1, WM gives significant discrepancies from the FEM/VCCT results. This shows that WM is only valid for the condition  $\beta = 1$ . Similar results are observed as the mode II fracture ratio increases, in Figures 8b and 8c (cases 2 and 3, respectively). Moreover, it is noticeable the limitation of WM to predict the fracture partitioning ratios on asymmetric cracks within the same material. This can be explained by the influence of the mode I and mode II coupling on the fracture energy.

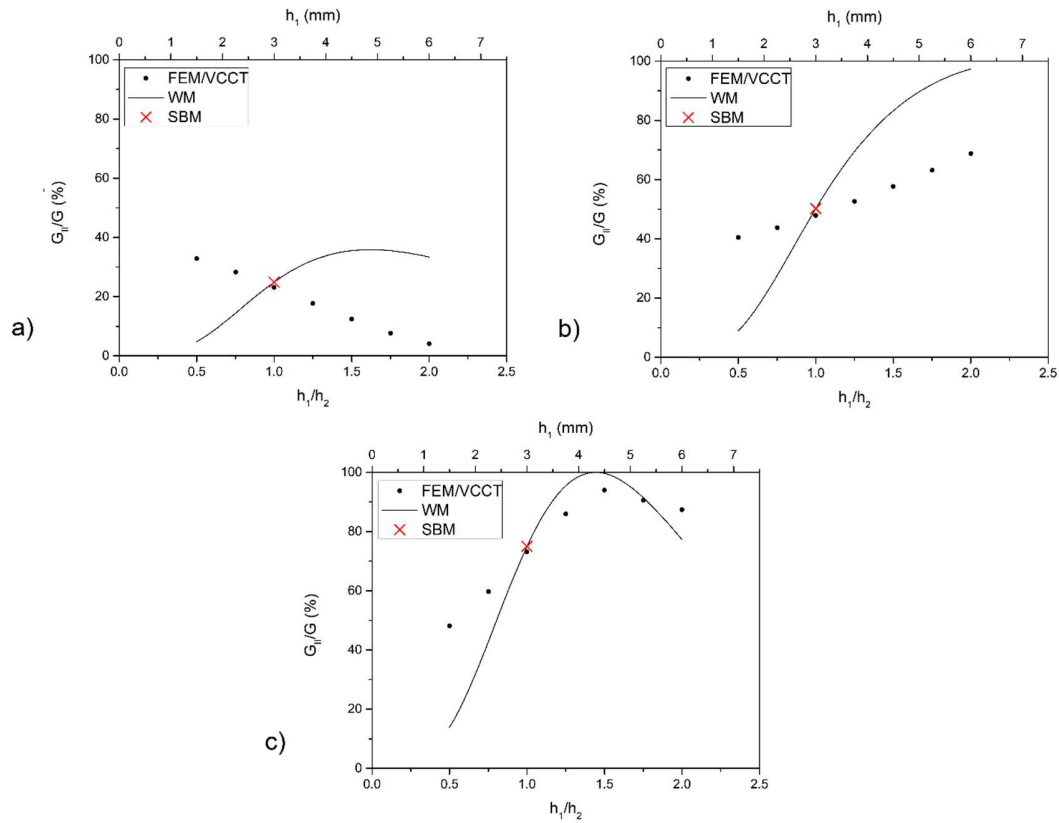


Figure 8. Fracture mode ratio with the variation of specimen thickness: cases (a) 1 – low, (b) 2 – intermediate and (c) 3 – high mode II [25].

Table 2 shows the results and errors of the analytical model in comparison with the numerical model for the condition of symmetric crack. Slight errors between -4.2% and -6.0% are observed in the calculation of the total fracture energy and between 2.6% and 7.6% in the fracture mode ratio. In the particular condition of a symmetric crack, literature suggests crack tip corrections in order to account for the effect of crack tip rotation under mode I [27] and mode II [29] fracture. The analytical method with the application of these correction factors presented insignificant errors for the calculation of the total fracture energy and errors lower than 4.0% for the fracture mode ratio – see Table 2. In both cases, the use of correction factors resulted in more accurate results. This shows that the effect of crack tip rotation during the experiments may have a non-negligible effect on the fracture behavior although the simple analytical model proved to be reliable.

Table 2. Results and errors of the analytical model in the condition of symmetric crack.

Case	Numerical model		Analytical model				Analytical model with crack tip corrections			
	G	G <sub>II</sub> /G	G	Erro	G <sub>II</sub> /G	Erro	G	Erro	G <sub>II</sub> /G	Erro
	(J/m <sup>2</sup> )	(%)	(J/m <sup>2</sup> )	r (%)	(%)	r (%)	(J/m <sup>2</sup> )	r (%)	(%)	r (%)
1	362.3	23.2	340.7	-6.0	24.9	7.6	364.7	0.6	24.1	4.0
2	87.7	47.9	83.1	-5.2	50.2	4.8	87.9	0.3	49.1	2.5
3	42.4	73.1	40.6	-4.2	75.0	2.6	42.5	0.2	74.1	1.4

#### 17.4.2.4. Bi-material crack

A second parametric study was carried out on a bi-material crack with asymmetric geometry. The upper arm has thickness ( $h_1$ ) of 2.12 mm and the lower arm has thickness ( $h_2$ ) of 3.0 mm. In order to verify the influence of the fracture mode ratio in the accuracy of the analytical methods, three different conditions were considered: low ( $c = 95$  mm), intermediate ( $c = 49$  mm) and high ( $c = 34$  mm) mode II ratio. Table 3 shows the three cases of bi-material crack. The upper arm elastic modulus ( $E_1$ ) is varied in a wide range of reasonable specimen materials applied to the MMB test. The lower arm has elastic modulus ( $E_2$ ) of 70 GPa and both arms have Poisson's ratio ( $\nu_1$  and  $\nu_2$ ) of 0.33. The crack length is kept at 50 mm and the test load ( $P$ ) is 100 N, likewise the previous cases.

Table 3. Study cases of bi-material crack.

Case	Lever length, c (mm)	$h_1$ (mm)	$h_2$ (mm)	$E_1$ (GPa)	$E_2$ (GPa)	$\nu_1; \nu_2$
4	95	2.12	3.0	$35 \leq E_1 \leq 210$	70	0.33
5	49	2.12	3.0	$35 \leq E_1 \leq 210$	70	0.33
6	34	2.12	3.0	$35 \leq E_1 \leq 210$	70	0.33

Analytical and numerical results of the total fracture energy (G) are presented in Figure 9. Both analytical methods give the same results for any material. Figures 9a, 9b and 9c show the three cases of low, intermediate and high mode II fracture, respectively. Both analytical

methods are in very good agreement with the FEM/VCCT results, hence, the analytical methods based on beam analysis provide reliable results of the total fracture energy on bi-material cracks.

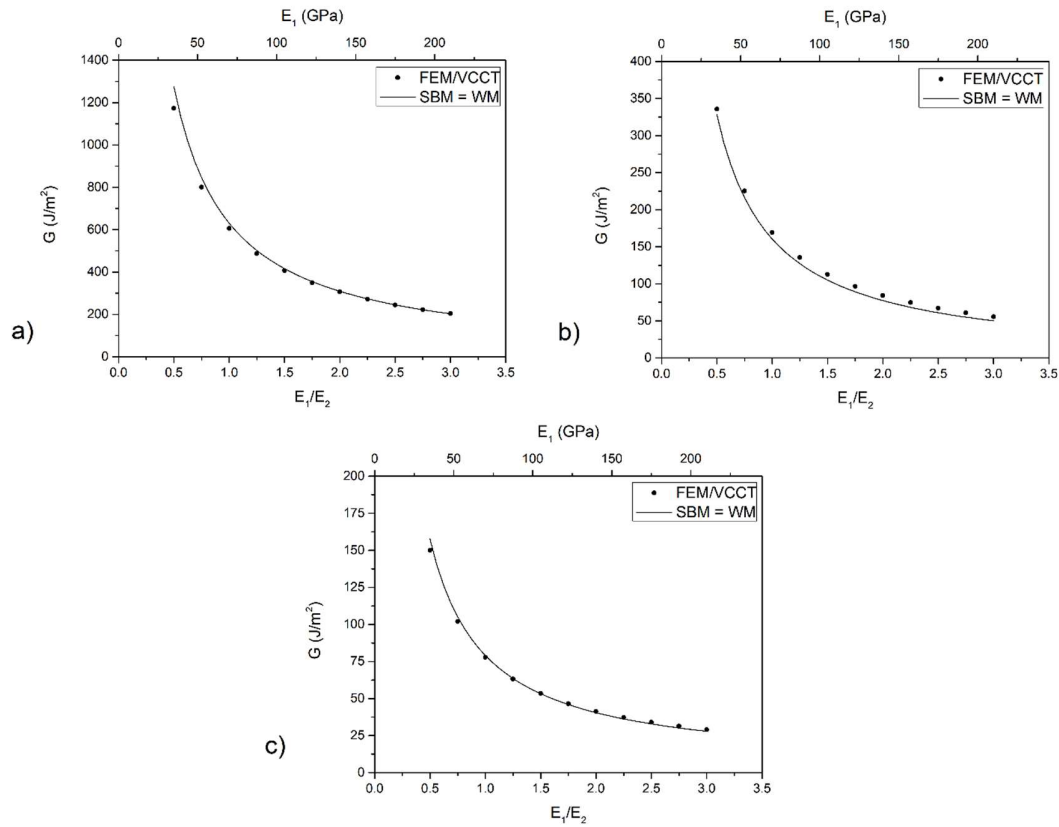


Figure 9. Total fracture energy with the variation of the specimen material: cases (a) 4 – low, (b) 5 – intermediate and (c) 6 – high mode II [25].

Figure 10 shows the analytical and numerical fracture mode ratio ( $G_{II}/G$ ). For the applied parameters, the strain-equivalent geometry ( $\beta = 1$ ) is achieved when  $E_1/E_2$  equals 2.0. In the case of low mode II (case 4), shown in Figure 10a, the SBM shows good agreement with the FEM/VCCT despite the remarkable asymmetry of the materials and geometry. However, as  $\beta$  differs from 1, WM gives significant discrepancies from the FEM/VCCT results. This shows that the analytical method based on beam analysis is only valid for when the strain-equivalence condition is respected. Similar results are observed as the mode II fracture ratio increases, presented in Figures 10b and 10c (cases 5 and 6, respectively). Moreover, it is shown once more that WM only predicts accurate fracture mode ratios when the condition of strain equivalence is satisfied ( $\beta = 1$ ). For any other geometry, the coupling effect between fracture modes is not taken into account and therefore incorrectly predicts the fracture mode ratios. The influence of the mode I and mode II coupling may have a large effect on the fracture mode of bi-material cracks. This reinforces the requirement of the strain-based design criterion for obtaining the correct partitioning ratio.

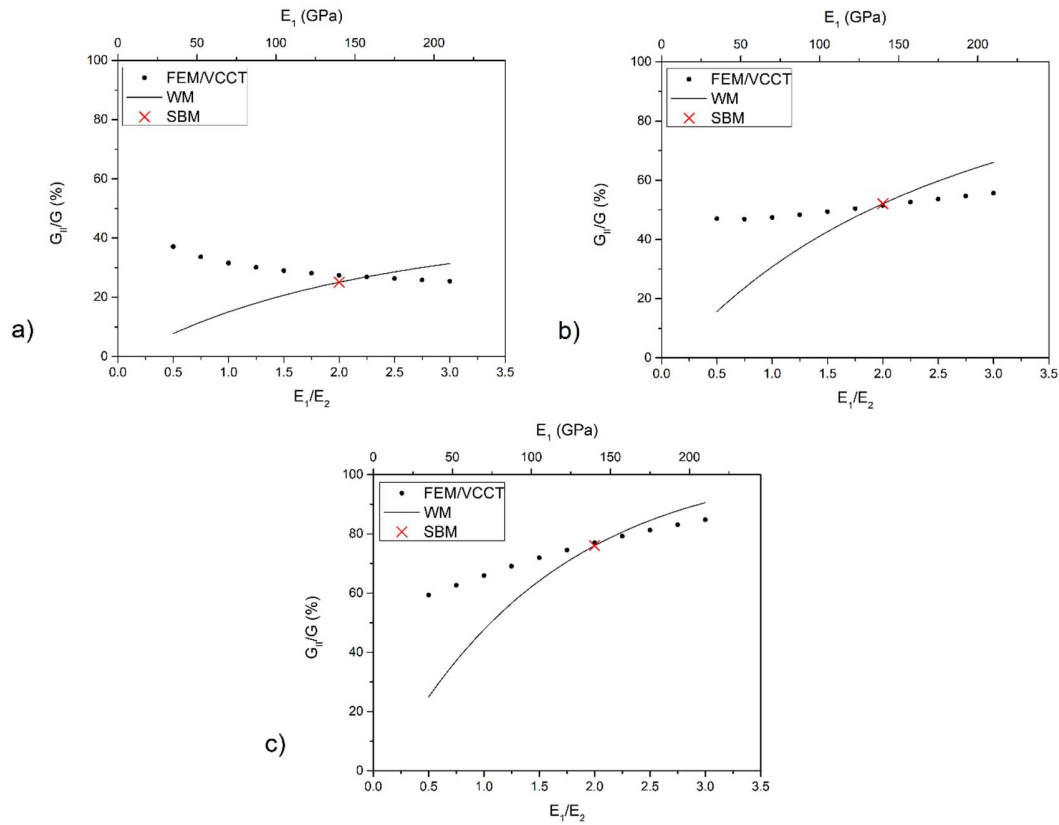


Figure 10. Fracture mode ratio with the variation of specimen material: cases (a) 4 – low, (b) 5 – intermediate and (c) 6 – high mode II [25].

Table 4 shows the results and errors of the analytical model in comparison with the numerical model for the particular condition of strain equivalence proposed in the SBM (see Equation 17.23). Errors between 1.0% and -8.1% are observed in the calculation of the total fracture energy and between 1.1% and -8.6% in the fracture mode ratio. These errors are in a similar degree as cases 1, 2 and 3 of symmetric condition, presented in Table 2. Therefore, it can be implied that the effect of crack tip rotation is also a major cause of the errors produced in cases 4, 5 and 6 of bi-material cracks using the SBM.

Table 4. Results and errors of the analytical model in the condition of strain equivalence.

Case	Numerical model		Strain-Based Method (SBM)			
	G (J/m <sup>2</sup> )	G <sub>II</sub> /G (%)	G (J/m <sup>2</sup> )	Error (%)	G <sub>II</sub> /G (%)	Error (%)
4	306.0	27.5	309.0	1.0	25.1	-8.6

5	84.2	51.5	77.4	-8.1	52.1	1.1
6	41.3	77.0	40.5	-2.0	76.0	-1.3

#### 17.4.2.5. Application of the SBM to composite-to-metal bonded joints

In order to evaluate the SBM and validate the previous numerical analysis, a test campaign has been conducted in which MMB tests were performed [25,33]. Composite-to-metal bonded joints were manufactured in thin and thick geometries. The geometry of the joint was designed to satisfy the criterion of strain equivalence ( $\beta = 1$ ). The mechanical properties of the materials are shown in Table 5.

Table 5. Mechanical properties of the materials.

Material	Elastic Modulus, $E_{11}$ (GPa)	Poisson's Ratio, $\nu_{12}$
Steel	200	0.27
Composite 0/90	46	0.24
Adhesive	2.25	0.38

Table 6 shows the test matrix. The half-span ( $L$ ) of the test is 70 mm and the initial crack length ( $a_0$ ) of 30 mm was obtained after bonding the end-blocks

Table 6. Test matrix.

Test	Specimen	Metal arm thickness, $h_1$ (mm)	Composite arm thickness, (mm)	Lever $h_2$ length, c (mm)	Lever center of gravity, $c_g$ (mm)	Lever weight, $P_g$ (kg)
1	thick	6.35	13.35	78	31	17.6
2	thick	6.35	13.35	78	31	17.6
3	thin	3.18	6.34	110	40	17.6



The total fracture energy and mode ratio were obtained at crack propagation using the SBM and the FEM. Figures 11a and 11b show the total fracture energy of Tests 1 and 2 in thick specimens. The SBM produced an error of 27.8% in the first measurement of crack propagation and reduces as the crack length increases, down to 11.4% in the last propagation point. The fracture mode ratio ( $G_{II}/G$ ) presented nearly constant values of 23.5% in the SBM and 21.5% in the FEM, as observed in Figure 11c. A constant fracture mode ratio is expected from the MMB test. The total fracture energy of Tests 3 and 4, in thin specimens, are presented in Figure 12a and 12b, respectively. In this geometry, the SBM produced an error of 13.2% in the first measurement of crack propagation and reduced as the crack length increases, down to 2.6% in the last propagation point. The analytical method produced more accurate results in the thin specimens compared to the thick ones. Moreover, the analytical solution showed more accuracy as the crack length increases due to the reduction of transverse shear effect that are not considered in the analytical model but can be significant in specimens with relatively large thickness. Finally, thin specimens presented a nearly constant fracture mode ratio ( $G_{II}/G$ ) of 19.8% from both the SBM and the FEM, as shown in Figure 12c. This shows the accuracy of the analytical solution and agrees with the results obtained from the parametric study in the previous section. Overall, the SBM gives reliable results for the calculation of the total fracture energy and mode ratio of bi-material crack as long as the shear effects are negligible.

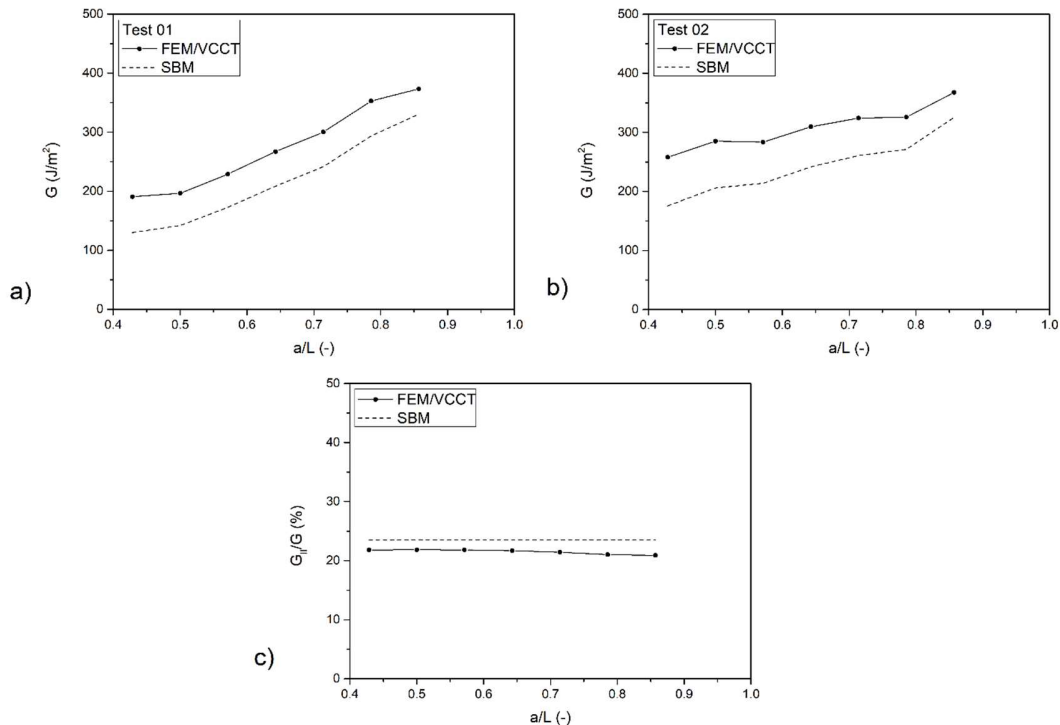


Figure 11. Total fracture energy and mode ratio of thick specimens [25].

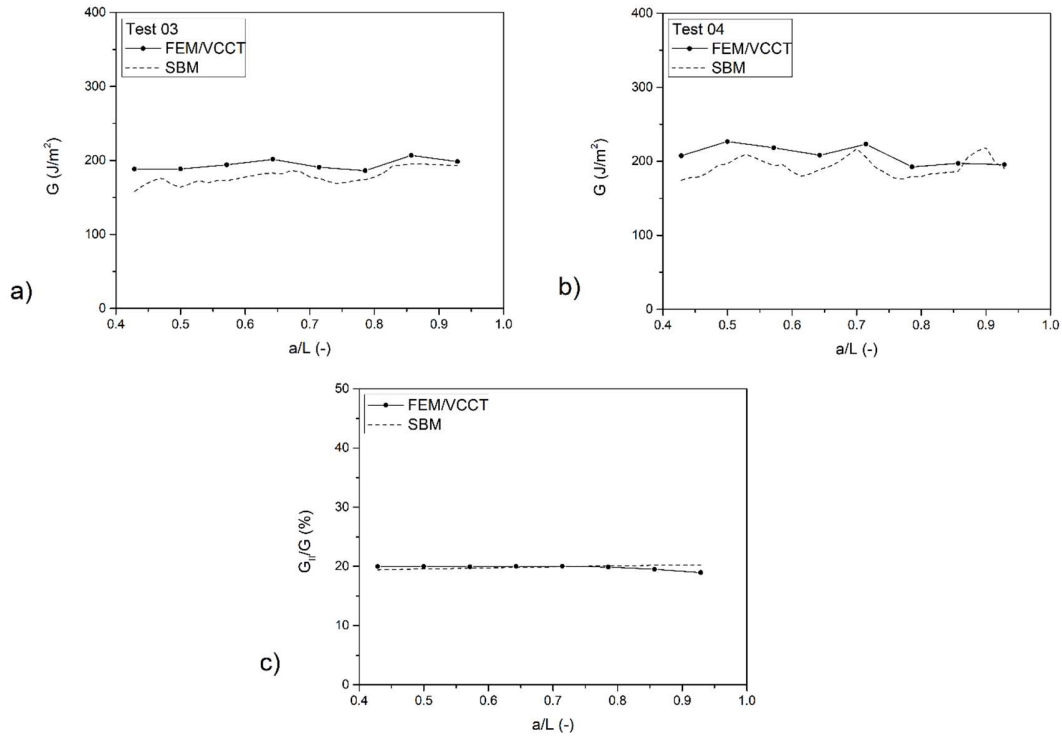


Figure 12. Total fracture energy and mode ratio of thin specimens [25].

## 17.5 Mixed-mode fracture behaviour

### 17.5.1 Crack stability

Crack stability is an important issue in the fracture testing of adhesively bonded joints as only for stable cracking can the change in applied force (and hence the compliance) be measured for a growing crack. A crack is unstable if an infinitesimal change in displacement is accompanied by a finite change in the crack length. The stability of crack growth may be judged from the sign of  $dG/da$ . Stable crack growth occurs if:

$$\frac{dG}{da} \leq 0 \quad (17.28)$$

The energy release rate was defined as the Irwin-Kies equation [8]:

$$G = \frac{P^2}{2B} \frac{dC}{da} \quad (17.29)$$

where  $P$  is the applied load and  $C$  is the compliance defined by  $\delta/P$  ( $\delta$  is the displacement). Considering the crack propagates very quickly with the displacement increment, the loading process is analogous to a condition of fixed grips. Eq. 17.29 can be transformed as:

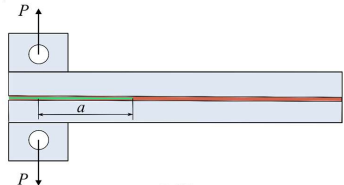
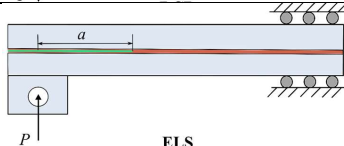
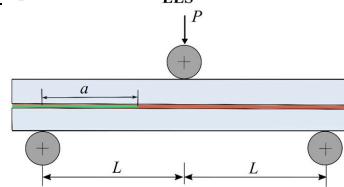
$$G = \frac{\delta^2}{2bC^2} \frac{dC}{da} \quad (17.30)$$

Combing the Eqs. (17.28) and (17.30) leads to the stability criterion fracture tests [21]

$$\frac{1}{2} C \frac{d^2C}{da^2} \frac{1}{(dC/da)^2} \leq 1 \quad (17.31)$$

Based on this theory, the stability criteria for a variety of fracture tests have been successfully derived, as documented in Table 7. Specimen pre-cracking is always recommended prior to a fracture test, as unstable crack growth can occur when testing the specimen directly from an insert. The resistance to crack initiation from an inserted release film (positioned in the adhesive layer during manufacture of the joint) may impose a greater initial crack resistance with  $(dG/da) > 0$ . Precracking the specimen so that the crack length can extend by a short distance from its initial length can improve stability.

Table 7. Specimen configuration and stability criteria for fracture testing of laminated composites and adhesive joints loaded in displacement control.

Fracture tests	Specimen configurations	Stability criteria	References
DCB & ADCB		Always stable	[30]
ELS		$a/L \geq 0.56$	[30]
3ENF		$a/L \geq 0.68$	[30]

4ENF		Always stable	[41]
MMB		$\frac{a}{L} \geq \left[ \frac{(c+L)^2}{4(3c-L)^2 + 3(c+L)^2} \right]^{\frac{1}{3}}$	[42]
MMF (or SLB)		$\frac{a}{L} \geq 0.49$	[43]
FRMM ( $h_1 = h_2$ )		$\frac{a}{L} \geq 0.41$	[30]
AFRMM ( $h_1 \neq h_2$ )		$\frac{a}{L} \geq \frac{\alpha}{1+\alpha} \left[ \frac{(1+\alpha)^2(1+\alpha^3)}{2((1+\alpha)^2 + 3\alpha^4)} \right]^{\frac{1}{3}}$ $\alpha = \frac{h_2}{h_1} = \frac{\text{Loaded arm}}{\text{Unloaded arm}}$	[44]
SPELT		$\frac{a}{L} \geq \left[ \frac{1+l/L}{1+\beta^*(\psi)} \right]^{\frac{1}{3}}$ $\psi$ is the nominal phase angle of loading, and $\beta^*(\psi)$ is dimensionless geometry parameter	[15]

However, unstable fracture behaviour can still occur despite the initial crack length satisfying the above criteria as crack stability is highly dependent upon the adhesive properties. Unstable fracture is more likely to occur in joints bonded with a brittle adhesive while joints bonded with a tougher adhesive tend to result in stable fracture behavior [45]. Moreover, crack stability is very sensitive to the mixed-mode ratio. While stable fracture can be obtained in the adhesively bonded CFRP under mode I and mode II loadings, unstable crack may appear in the mixed mode I/II loading. Researchers, e.g. [46], also reported that the crack in glass epoxy laminates bonded with Redux 420 epoxy adhesive propagated very rapidly and unstably under mode I dominated loading, whereas the propagation became more stable under mode II dominated loading, when the fracture resistance was greater.

The fracture behaviour of asymmetric specimens suggests the size of the cohesive zone may be a critical factor governing the stability of crack growth in adhesive joints [44]. In the AFRMM joints loaded via the thinner arm (mode I dominated), the crack was found to grow stably within the adhesive. In contrast, in the case loaded with the thicker arm (mode II dominated) the response became rather unstable, with the crack propagating to the clamping point abruptly, associated with a change in the type of failure from cohesive in the adhesive layer to interlaminar in the CFRP substrates. The FEA simulation suggests extensive damage accumulated ahead of the crack tip in the AFRMM specimen loaded via the thicker arm, leading to much longer cohesive zones than those loaded inversely. In addition, the length of the cohesive zone decreased rapidly after reaching a maximum. This abrupt reduction could explain the unstable nature of these tests.

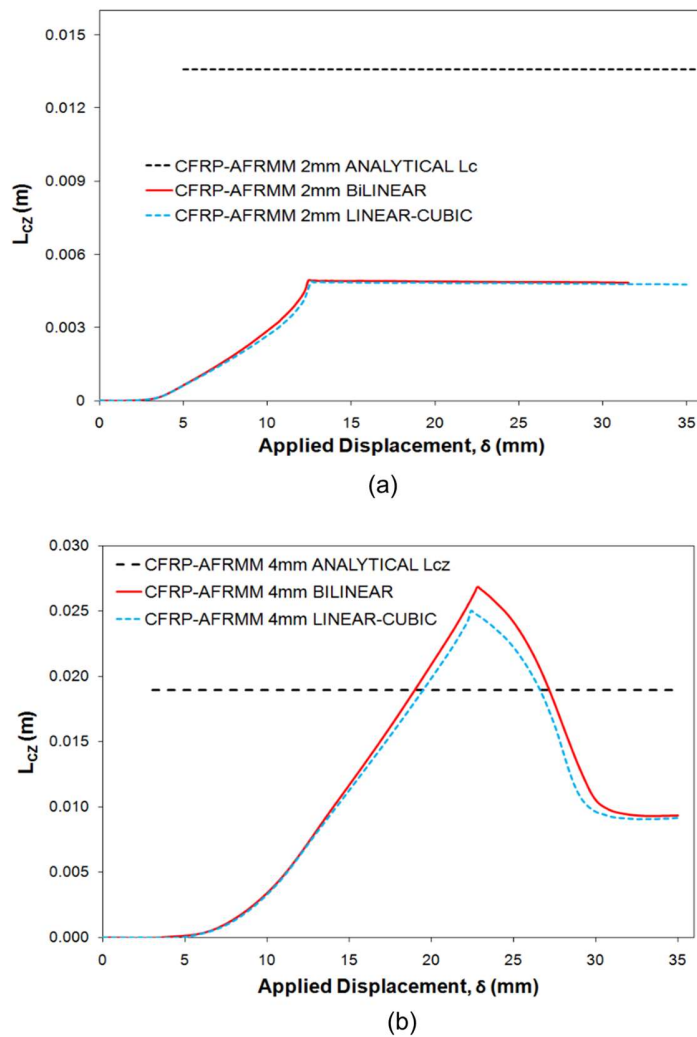


Figure 13. The cohesive zone length as a function of applied displacement in AFRMM specimens loaded at (a) the thinnest and (b) the thickest arms from FEA simulations, assuming a bilinear and a linear cubic traction separation law and from an analytical method. The analytical estimate was calculated by adding the contributions of the pure mode components of  $G_{IC}^m$  and  $G_{IIC}^m$ , i.e.  $l_{CZ}^m = l_{CZ,I}(G_{IC}^m) + l_{CZ,II}(G_{IIC}^m)$  [44].

## 17.5.2 Crack paths

Crack path is a major concern for the fracture analysis of layered materials. Due to the existence of elastic mismatch, microdefects and residual stresses on the interface, it is quite challenging to predict the crack paths analytically. Fleck et al. [47] have established LEFM theories to predict the crack path in adhesively bonded structures under mode I with finite mode II loading, based on the experimentally established fact that a crack advancing continuously in an isotropic, homogeneous, brittle solid selects a trajectory where local stress intensity factor  $K_{II} = 0$ . The remote field in the asymptotic problem in Figure 14 is specified by  $K_I^\infty$ ,  $K_{II}^\infty$ ,  $T^\infty$  and  $\sigma^0$ , where  $K_I^\infty$  and  $K_{II}^\infty$  are the remote values of the mode I and mode II stress intensity factors,  $T^\infty$  is the remote T-stress and  $\sigma^0$  is the  $\sigma_{xx}$  component of residual stress pre-existing in the adhesive due to thermal mismatch or other sources. The solution to the elasticity problem (as shown in Figure 14) provides the local  $K_I$ ,  $K_{II}$  and  $T$  at the crack tip within the layer, and is given by the following equations, with  $c_I$  and  $c_{II}$  and  $\phi_H(\alpha, \beta) + \omega(\alpha, \beta)$  being tabulated in [47].

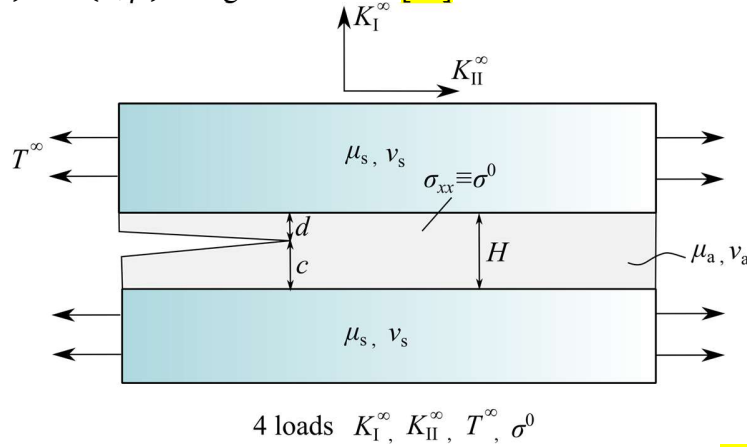


Figure 14. The elasticity problem (redraw after Fleck et al. [47])

The local ( $K_I$ ,  $K_{II}$ ) depends only on the remote loads  $K_I^\infty$  and  $K_{II}^\infty$ , and the two sets are connected by the energy release rate due to conservation of the  $J$ -integral:

$$K_I + iK_{II} = \left( \frac{1 - \alpha}{1 + \alpha} \right)^{1/2} (K_I^\infty + K_{II}^\infty) e^{i\phi} \quad (17.32)$$

where  $\phi$  can be interpreted as a phase angle shift between the remote and local stress intensities,  $\phi \equiv \tan^{-1}(K_{II}/K_I) - \tan^{-1}(K_{II}^\infty/K_I^\infty)$ .  $\phi$  is only a function of structures, i.e.

$\phi = \phi(c/H, \alpha, \beta)$ :

$$\phi = \varepsilon \ln \left( \frac{H - c}{c} \right) + 2 \left( \frac{c}{H} - \frac{1}{2} \right) [\phi_H(\alpha, \beta) + \omega(\alpha, \beta)] \quad (17.33)$$

where  $\alpha, \beta$  are Dundurs elastic mismatch parameters,  $\varepsilon = (1/2\pi) \ln[(1 - \beta)/(1 + \beta)]$ , the function  $\omega(\alpha, \beta)$  is tabulated in [48] and  $\phi_H$  is given in Hutchinson et al. [49].

The local T-stress depends linearly on all four loading parameters.

$$T = \frac{1-\alpha}{1+\alpha} T^\infty + \sigma^0 + c_I \frac{K_I^\infty}{\sqrt{H}} + c_{II} \frac{K_{II}^\infty}{\sqrt{H}} \quad (17.34)$$

where the two non-dimensional functions,  $c_I(c/H, \alpha, \beta)$  and  $c_{II}(c/H, \alpha, \beta)$  are given in [47].

A necessary condition for the existence of a straight path within the layer is the location of a path with  $K_{II} = 0$ . Such a path will only be stable if  $T < 0$ . Symmetry indicates that a crack along the centre line of a layer joining identical materials and subject to remote pure mode I loading will be under pure mode I locally. When the base specimen carries some mode II in addition to mode I, the crack may find a pure mode I path off the centre line. When the mode II component is sufficiently large, typically  $\tan^{-1}(K_{II}^\infty/K_I^\infty) \geq 15^\circ$ , the crack runs along the epoxy/aluminium interface and the measured  $G_c$  is the mode dependent interfacial fracture energy. For values of  $K_{II}^\infty/K_I^\infty$  outside the range of possible retention of the crack within the layer (e.g.,  $\tan^{-1}(K_{II}^\infty/K_I^\infty)$  greater than 0-10 degrees depending on the mismatch), the crack will be driven toward one interface or the other- toward the lower interface if  $K_{II}^\infty > 0$  and toward the upper if  $K_{II}^\infty < 0$  [50].

For tough adhesive systems in which LEFM may not still be valid, there exists considerable experimental evidence that suggests that the type of loading affects the crack propagation path (i.e. loci of failure). Mixed mode I/II tends to drive the crack towards the interface of the adhesive joint. For instance, Blackman et al. [51] reported that the adhesively bonded CFRP joints loaded in mixed-mode ( $G_I/G_{II} = 4/3$ ) failed via a delamination mechanism, with the crack switching from the position of the cohesive pre-crack to a path within the composite substrate, in contrast to the cohesive failure that occurred under the pure mode I or mode II loading. Blackman et al. pointed out that this type of failure was related to the transverse tensile stresses ( $\sigma_{yy}$ ) exerted on the CFRP substrates. If the transverse stresses exceeded the transverse strength ( $\sigma_{yyc}$ ), fracture could take place in the composite arms. An approximation to the transverse stress,  $\sigma_{yy}$ , on a single substrate for the loading modes was developed, which indicated that the greatest transverse stresses were produced by mixed-mode loading using the FRMM specimen, which has only a single arm being loaded.

### 17.5.3 Failure envelopes

A comprehensive review of failure envelopes, including information on the type of responses modelled in each case, can be found in [52]. These criteria were initially developed for composite materials, but there is much evidence showing they are also valid for adhesive joints. The most widely used empirical criteria for the failure of adhesive joints are the power criterion [53] (Eq. 17.35) and the B-K criterion [40] (Eq. 17.36). Both criteria were implemented in several commercial finite element analysis codes.



$$\left(\frac{G_I}{G_{Ic}}\right)^m + \left(\frac{G_{II}}{G_{IIc}}\right)^n = 1 \quad (17.35)$$

$$G_{I/IIc} = G_{Ic} + (G_{IIc} - G_{Ic}) \left(\frac{G_{II}}{G_I + G_{II}}\right)^n \quad (17.36)$$

Figure 15 presents the fracture toughness as a function of the mode-mixity ( $G_{II}/G$ ) for the unidirectionally reinforced carbon fibre composite substrates bonded with the epoxy adhesive, 3M-D460 [54]. The power law captured the failure envelope of the adhesive joints when the exponents  $m = 0.63$  and  $n = 1.43$ , and indeed the power law criterion with a single exponent of 1.0 has been able to provide a satisfactory fit.

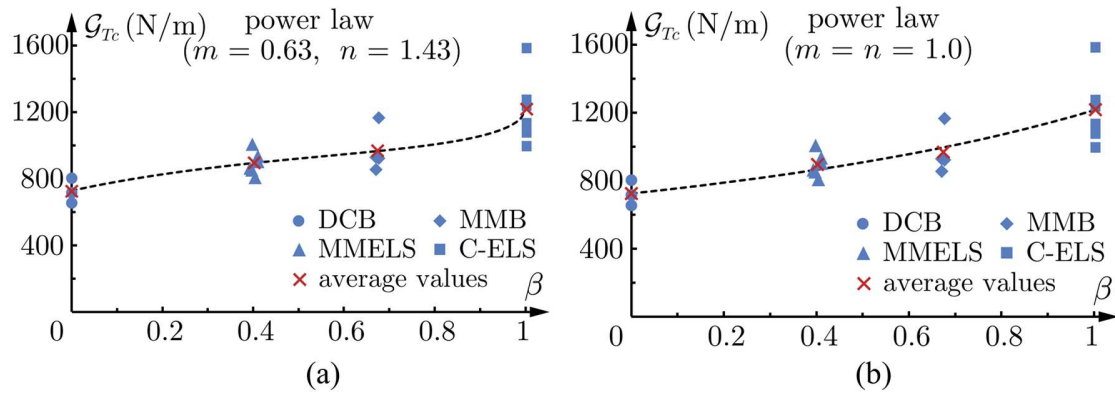


Figure 15. Values of  $G$ -total ( $G_{Tc}$ ) as a function of mixed-mode ratio  $\beta = G_{II}/G_{Tc}$  for: (a) exponents  $m = 0.63$  and  $n = 1.43$  and (b) a single exponent of 1.0 [54].

It has been reported that the B-K failure criterion successfully described the failure behaviour of adhesive joints employing metallic substrates. Figure 16 shows the fracture toughness of a crash resistant epoxy adhesive SikaPowers-498 measured under various values of mixed-mode ratio using TDCB and MMB tests [55]. Figure 17 gives another example of the fracture toughness of Araldite-2015 bonded metallic joints determined by DCB and MMB tests [56]. For both sets of experimental data, there was a steady increase in the fracture resistance as the mixed-mode ratio increased from 0 (pure mode I) to 1 (pure mode II). The B-K model captured the fracture behaviour as a function of mixed-mode ratio closely.

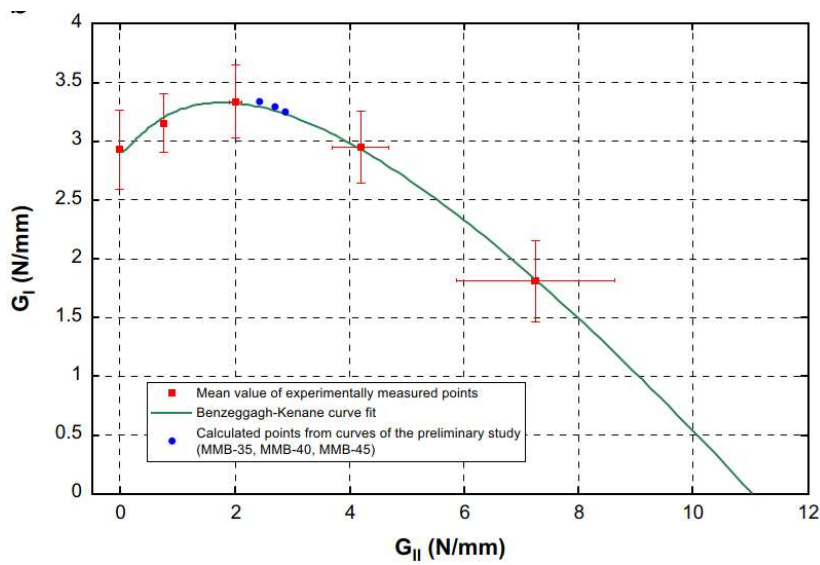


Figure 16. Mixed-mode fracture data measured on joints employing metallic substrates bonded with SikaPower 498 adhesive, fitted using the B-K criterion [55].

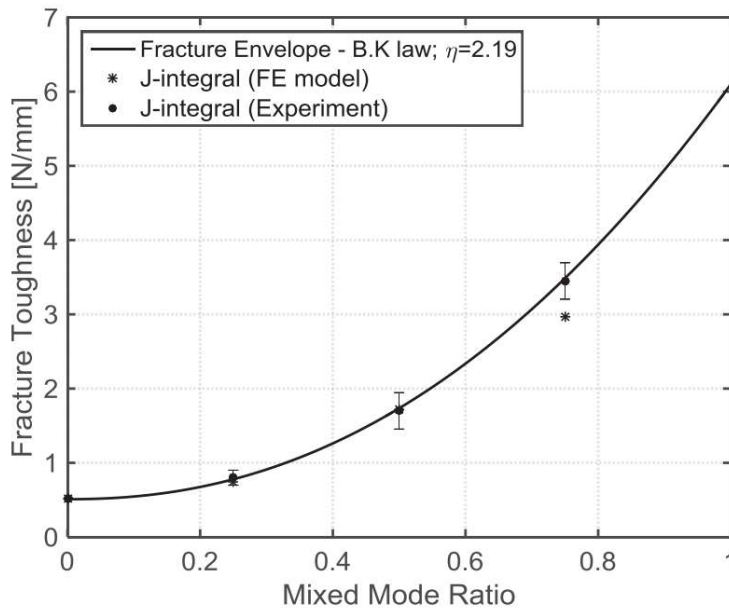


Figure 17. Mixed-mode fracture data measured on joints employing metallic substrates bonded with Araldite 2015 adhesive, fitted using the B-K criterion [56].

The B-K model requires that the fracture toughness value always increases as the contribution of mode II is increased, i.e.  $G_{Ic} < G_{I/IIc} < G_{IIc}$ , however, such a monotonically increasing trend is not always measured for adhesive joints. Figure 18 presents B-K criteria constructed for joints bonded with the toughened automotive adhesive XD4600 under quasi-static loading [57]. Different values of  $\eta$  were used for the B-K criterion, but it was not possible for this model to fit the low mixed-mode I/II values produced when a switch in crack propagation path, to interfacial failure or composite delamination, occurred. Clearly, these joints which showed substrate delamination under mixed mode loading did

not comply with the “monotonic increase” requirement. Similar non-monotonic behaviour caused by the failure mechanism changing from cohesive (in the adhesive) to adhesive (on the carrier cloth/adhesive interface) under the mixed mode loading was also reported by Dillard et al. [58]. However, the Charalambides, Kinloch, Wang and Williams (CKWW) criterion [59] (in Eq. 17.37) was found to be capable of capturing the non-monotonic fracture envelope due to the criterion having two fitting parameters,  $\kappa$  and  $\varphi$ , which enabled the fitting of more complex failure envelopes.

$$\left(\frac{G_I}{G_{Ic}} - 1\right)\left(\frac{G_{II}}{G_{IIc}} - 1\right) - \left[\kappa + \varphi\left(\frac{G_I}{G_I + G_{II}}\right)\right]\left(\frac{G_I}{G_{Ic}}\right)\left(\frac{G_{II}}{G_{IIc}}\right) = 0 \quad (17.37)$$

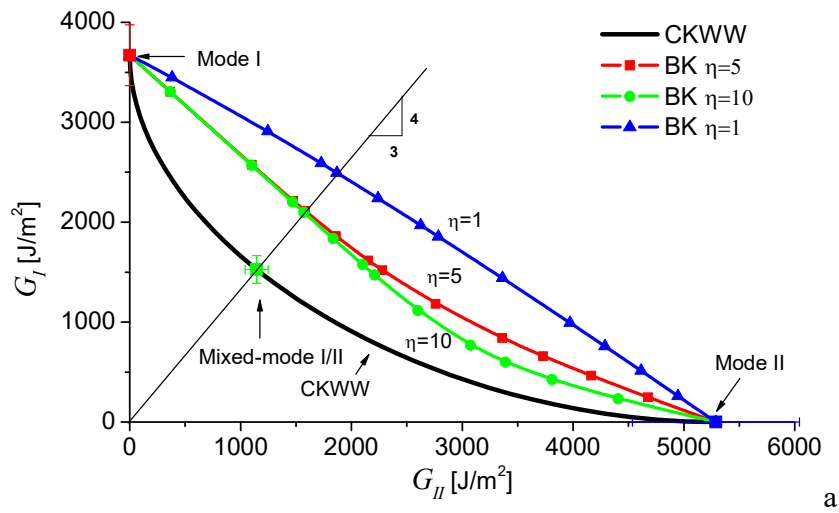


Figure 18. Comparison of the use of the CKWW and BK criteria for construction of the failure envelope for joints bonded with a toughened automotive adhesive XD4600, when substrate delamination occurred [57].

Figure 19 displays another example of fitting failure envelopes [60]. The fracture toughness determined at the point of the maximum load, in which the discrete value for  $\beta = 0.25$  violates a monotonic trend, i.e., in the range of  $\beta < 0.25$  the  $G_c$  decreases with increasing mixity but when  $\beta > 0.25$  it increases. The B-K criterion and the power law with  $\alpha_1 = \alpha_2 = 1$ , both of which require a monotonical increase in  $G_c$  values did not yield good approximation of the  $G_c$  value at  $\beta = 0.25$ . Instead, the best fit of the  $G_c$  values is obtained by the second order polynomial, clearly captured the transition in the  $G_c$  value at  $\beta = 0.25$ .

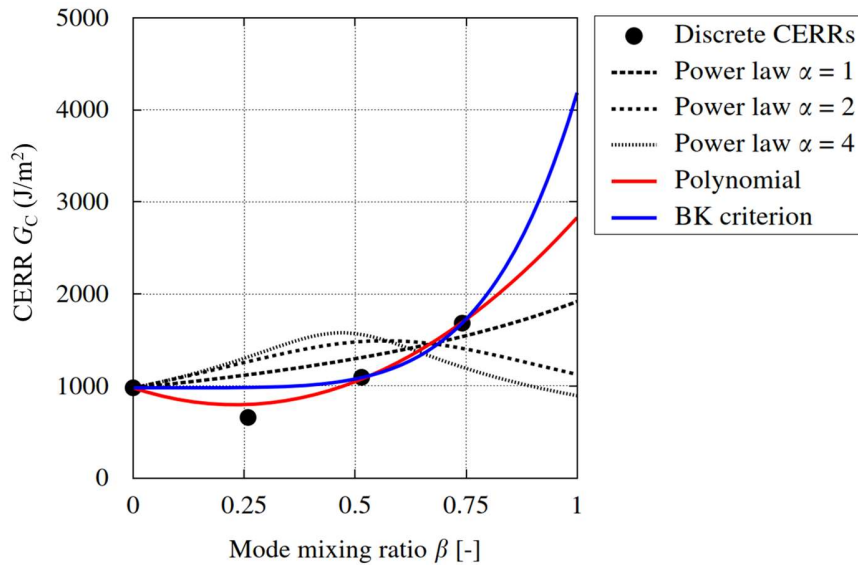


Figure 19. Comparison of the use of the various failure criteria for construction of the failure envelopes for unidirectional Hexcel IM7/ 8552 carbon/epoxy composite bonded with film adhesive Cytec FM 300 M [60].

## 17.6 Conclusions and outlook

The characterization of fracture in adhesively bonded joints under mixed-mode (I/II) loading conditions has been discussed. While standardised tests for adhesive joints in mixed-mode are not yet available, much use has been made of methods developed initially for composite laminates such as the mixed-mode bend test, the fixed-ratio mixed mode test with both symmetric and asymmetric geometry and the asymmetric double cantilever beam. Most analyses utilize LEFM and corrected beam theory to determine the fracture resistance as a function of mixed-mode ratio.

Efforts to partition the mixed-mode (I/II) fracture resistance into pure mode components have typically followed either a local singular field approach or a global approach. The application of these partitioning strategies to adhesively bonded joints has led to the conclusion that neither strategy works well across the wide spectrum of adhesives in common usage. The local singular field approach has been shown to be more suitable when brittle adhesives are employed (when the damage zone ahead of the crack tip is very limited in size.) Conversely, the global partitioning approach is shown to be more suitable when toughened adhesives are employed (when the damage zone ahead of the crack tip is larger.) A semi-analytical cohesive zone analysis has been shown to work equally well across the wide spectrum of adhesives in use. This approach utilizes a singularity factor which scales from the local to the global solutions and therefore has wide applicability.

The limitations of global partitioning have been further explored with the goal to design and analyse adhesive joints with dissimilar adherends - a bi-material interface joint. The definition of mode I loading in the mixed-mode case has been modified by the incorporation of a longitudinal strain criteria. Further, the coupling between the modes I and II components and their contribution to the total mixed-mode fracture energy has been

considered and the technique has been verified numerically. Such an approach offers advantages for the design of adhesive joints with dissimilar adherends and their analysis.

Finally, the issues of crack stability, crack path selection and failure envelopes for mixed-mode loading were considered.

In terms of future trends, as adhesives become more highly toughened they present larger damage zones at the crack tip and the use of LEFM becomes increasingly inaccurate. As such, non-linear methods e.g. the  $J$ -integral (as discussed in Chapter 17 (Marzi)), will increasingly be required. Also, developments in experimental techniques such as digital image correlation which can be used to simultaneously track the crack growth, measure the traction-separation law and determine  $J_c$  will become more popular. Also, as materials become more complex, especially layered or laminated materials which can be incorporated into adhesively bonded joints, then there is significant scope to design more fracture resistant systems where knowledge of the failure paths under mixed-mode loading can be exploited.

## 17.7 Chapter References

- [1] Kinloch AJ. Adhesion and Adhesives: Science and Technology. London: Chapman & Hall; 1987.
- [2] Da Silva LFM, Öchsner A, Adams RD. Handbook of Adhesion Technology. Heidelberg: Springer-Verlag Berlin Heidelberg; 2011.
- [3] Ripling EJ, Mostovoy S, Patrick RL. Measuring fracture toughness of adhesive joints. Mater Res Stand (ASTM Bull) 1964;4:129–34.
- [4] ASTM D3433-93, Standard test method for fracture strength in cleavage of adhesives in bonded metal joints. 1993.
- [5] Liechti KM, Freda T. On the use of laminated beams for the determination of pure and mixed-mode fracture properties of structural adhesives. J Adhes 1989;28:145–69.
- [6] Li S, Wang J, Thouless MD. The effects of shear on delamination in layered materials. J Mech Phys Solids 2004;52:193–214.
- [7] Singh HK, Chakraborty A, Frazier CE, Dillard DA. Mixed mode fracture testing of adhesively bonded wood specimens using a dual actuator load frame. Holzforschung 2010;64:353–61.
- [8] Irwin GR, Kies JA. Critical energy release rate analysis of fracture strength of large welded structures. Weld J 1954;33:193–198.
- [9] Chaves FJP, Silva LFM, Moura MFSF De, Dillard DA, Esteves C, Chaves FJP, et al. Fracture Mechanics Tests in Adhesively Bonded Joints : A Literature Review 2014; 8464.
- [10] Sørensen BF, Brethe P, Skov-Hansen P. Controlled Crack Growth in Ceramics: The DCB Specimen Loaded with Pure Moments. J Eur Ceram Soc 1996;16:1021–5.
- [11] Carlsson LA, Gillespie JW, Pipes RB. On the Analysis and Design of the End Notched Flexure (ENF) Specimen for Mode II Testing. J Compos Mater 1986;20:594–604.
- [12] Blackman BRK, Kinloch AJ, Paraschi M. The determination of the mode II adhesive

- fracture resistance,  $G_{IIC}$ , of structural adhesive joints: An effective crack length approach. *Eng Fract Mech* 2005;72:877–97.
- [13] Reeder JR, Crews JH. Nonlinear analysis and redesign of the Mixed-Mode bending Delamination test. Langley Research Center Hampton, Virginia: 1991.
- [14] Arcan M, Hashin Z, Voloshin A. A method to produce uniform plane-stress states with applications to fiber-reinforced materials - A specially designed specimen yields material properties under pure shear or uniform plane-stress conditions. *Exp Mech* 1978;18:141–6.
- [15] Fernlund G, Spelt JK. Mixed-mode fracture characterization of adhesive joints. *Compos Sci Technol* 1994;50:441–9.
- [16] ASTM: D6671M. Standard Test Method for Mixed Mode I-Mode II Interlaminar Fracture Toughness of Unidirectional Fiber Reinforced Polymer Matrix Composites. 2006.
- [17] Costa M, Carbas R, Marques E, Viana G, da Silva LFM. An apparatus for mixed-mode fracture characterization of adhesive joints. *Theor Appl Fract Mech* 2017;91:94–102.
- [18] Lai YH, Rakestraw MD, Dillard DA. The cracked lap shear specimen revisited - A closed form solution. *Int J Solids Struct* 1996;33:1725–43.
- [19] Johnson WS. Stress analysis of the cracked-lap-shear specimen - An ASTM round-robin. *J Test Eval* 1987;15:303–24.
- [20] Williams JG. The fracture mechanics of delamination tests. *J Strain Anal* 1989;24:207–14.
- [21] Williams JG. On the calculation of energy release rates for cracked laminates. *Int J Fract* 1988;36:101–19.
- [22] Conroy M, Kinloch AJ, Williams JG, Ivankovic A. Mixed mode partitioning of beam-like geometries: A damage dependent solution. *Eng Fract Mech* 2015;149:351–67.
- [23] Álvarez D, Guild FJ, Kinloch AJ, Blackman BRK. Partitioning of mixed-mode fracture in adhesively-bonded joints: experimental studies. *Eng Fract Mech* 2018;203:224–39.
- [24] Davidson BD, Gharibian SJ, Yu L. Evaluation of energy release rate-based approaches for predicting delamination growth in laminated composites. *Int J Fract* 2000;105:343–65.
- [25] Arouche MM, Teixeira de Freitas S, de Barros S. Evaluation of the strain-based partitioning method for mixed-mode I+II fracture of bi-material cracks. *J Adhes* 2022;98:577–605.
- [26] Williams JG. Large Displacement and End Block Effects in the “DCB” Interlaminar Test in Modes I and II. *J Compos Mater* 1987;21:330–47.
- [27] Williams JG. End corrections for orthotropic DCB specimens. *Compos Sci Technol* 1989;35:367–76.
- [28] Kanninen MF. A dynamic analysis of unstable crack propagation and arrest in the DCB test specimen. *Int J Fract* 1974;10:415–30.
- [29] Wang Y, Williams JG. Corrections for mode II fracture toughness specimens of composites materials. *Compos Sci Technol* 1992;43:251–6.
- [30] Hashemi S, Kinloch AJ, Williams JG. The analysis of interlaminar fracture in uniaxial fibre-polymer composites. *Proc R Soc London A Math Phys Sci*

- 1990;427:173–99.
- [31] Ducept F, Davies P, Gamby D. An experimental study to validate tests used to determine mixed mode failure criteria of glass/epoxy composites. *Compos Part A Appl Sci Manuf* 1997;28:719–29.
  - [32] Ducept F, Gamby D, Davies P. A mixed-mode failure criterion derived from tests on symmetric and asymmetric specimens. *Compos Sci Technol* 1999;59:609–19.
  - [33] Arouche MM, Wang W, Teixeira de Freitas S, de Barros S. Strain-based methodology for mixed-mode I+II fracture: A new partitioning method for bi-material adhesively bonded joints. *J Adhes* 2019;95:385–404.
  - [34] Ouyang Z, Ji G, Li G. On approximately realizing and characterizing pure mode-I interface fracture between bonded dissimilar materials. *J Appl Mech Trans ASME* 2011;78:1–12.
  - [35] Wang W, Lopes Fernandes R, Teixeira De Freitas S, Zarouchas D, Benedictus R. How pure mode I can be obtained in bi-material bonded DCB joints: A longitudinal strain-based criterion. *Compos Part B Eng* 2018;153:137–48.
  - [36] Mollón V, Bonhomme J, Argüelles A, Viña J. Influence of the crack plane asymmetry over G II results in carbon epoxy ENF specimens. *Compos Struct* 2012;94:1187–91.
  - [37] Reeder JR, Crews JH. Redesign of the Mixed-Mode Bending Delamination Test to Reduce Nonlinear Effects. *J Compos Technol Res* 1992;14:12–9.
  - [38] Reeder JR. A Bilinear Failure Criterion for Mixed-Mode Delamination. *Compos. Mater. Test. Des. (Vol 11)*, ASTM STP 1206, Philadelphia: 1993, p. 302–22.
  - [39] Chen JH, Sernow R, Schulz E, Hinrichsen G. Modification of the mixed-mode bending test apparatus. *Compos Part A Appl Sci Manuf* 1999;30:871–7.
  - [40] Benzeggagh ML, Kenane M. Measurement of mixed-mode delamination fracture toughness of unidirectional glass/epoxy composites with mixed-mode bending apparatus. *Compos Sci Technol* 1996;56:439–49.
  - [41] Schuecker C, Davidson BD. Evaluation of the accuracy of the four-point bend end-notched flexure test for mode II delamination toughness determination. *Compos Sci Technol* 2000;60:2137–46.
  - [42] Yum YJ, You AH. Pure mode I, II and mixed mode interlaminar fracture of graphite/epoxy composite materials. *J Reinf Plast Compos* 2001;20:794–808.
  - [43] Szekrényes A. Crack stability of fracture specimens used to test unidirectional fiber reinforced material. *Exp Mech* 2010;50:473–82.
  - [44] Alvarez Feito D. Fracture mechanics of carbon fibre reinforced plastics to Ti-alloy adhesive joints. PhD Thesis, Imperial College London, 2012.
  - [45] Sun F, Blackman BRK. A DIC method to determine the Mode I energy release rate  $G$ , the  $J$ -integral and the traction-separation law simultaneously for adhesive joints. *Eng Fract Mech* 2020;234:107097.
  - [46] Ducept F, Davies P, Gamby D. Mixed mode failure criteria for a glass/epoxy composite and an adhesively bonded composite/composite joint. *Int J Adhes Adhes* 2000;20:233–44.
  - [47] Fleck NA, Hutchinson JW, Suo Z. Crack path selection in a brittle adhesive layer. *Int J Solids Struct* 1991;27:1683–703.
  - [48] Huang R, Suo Z, Prevost JH, Nix WD. Inhomogeneous deformation in metallic glasses. *J Mech Phys Solids* 2002;50:1011–27.

- [49] Hutchinson JW, Mear ME, Rice JR. Crack paralleling an interface between dissimilar materials. *J Appl Mech Trans ASME* 1987;54:828–32.
- [50] Hutchinson JW, Suo Z. Mixed Mode Cracking in Layered Materials. vol. 29. 1991.
- [51] Blackman BRK, Kinloch AJ, Rodriguez-Sanchez FS, Teo WS. The fracture behaviour of adhesively-bonded composite joints : Effects of rate of test and mode of loading. *Int J Solids Struct* 2012;49:1434–52.
- [52] Reeder JR. 3-D Mixed Mode Delamination Fracture Criteria - An Experimentalist's Perspective, in: B. Sankar, A. Waas, M. Hyer (Eds.), *Damage in Composites*, Destech Publications, Lancaster, PA, 2013, pp. 129–146.
- [53] Wu EM, Reuter RC. Crack extension in fiberglass reinforced plastics. University of Illinois, Urbana, IL, Report No. 275, 1965.
- [54] Simon I, Banks-Sills L. Mixed mode I/II interlaminar initiation fracture toughness of a secondary bonded pultrusion composite laminate. *Theor Appl Fract Mech* 2021;114: 103018.
- [55] Stamoulis G, Carrere N, Cognard JY, Davies P, Badulescu C. On the experimental mixed-mode failure of adhesively bonded metallic joints. *Int J Adhes Adhes* 2014;51:148–58.
- [56] Sadeghi MZ, Zimmermann J, Gabener A, Schroeder KU. The applicability of J-integral approach in the determination of mixed-mode fracture energy in a ductile adhesive. *Int J Adhes Adhes* 2018;83:2–8.
- [57] Rodriguez-Sanchez FS. *Fracture Behaviour of Automotive Adhesive Joints*. Imperial College London, PhD 2008.
- [58] Dillard DA, Singh HK, Pohlit DJ, Starbuck JM. Observations of decreased fracture toughness for mixed mode fracture testing of adhesively bonded joints. *J Adhes Sci Technol* 2009;23:1515–30.
- [59] Charalambides M, Kinloch AJ, Wang Y, Williams JG. On the analysis of mixed-mode failure. *Int J Fract* 1992;54:269–91.
- [60] Balzani C, Wagner W, Wilckens D, Degenhardt R, Büsing S, Reimerdes HG. Adhesive joints in composite laminates - A combined numerical/experimental estimate of critical energy release rates. *Int J Adhes Adhes* 2012;32:23–38.